pp 1208–1235. © The Author(s) 2020. Published by Cambridge University Press on behalf of Royal Aeronautical Society
doi:10.1017/aer.2020.24

Minimising induced drag with weight distribution, lift distribution, wingspan, and wing-structure weight

W.F. Phillips, D.F. Hunsaker and J.D. Taylor
doug.hunsaker@usu.edu
Utah State University
Logan, Utah
USA

ABSTRACT

Because the wing-structure weight required to support the critical wing section bending moments is a function of wingspan, net weight, weight distribution, and lift distribution, there exists an optimum wingspan and wing-structure weight for any fixed net weight, weight distribution, and lift distribution, which minimises the induced drag in steady level flight. Analytic solutions for the optimum wingspan and wing-structure weight are presented for rectangular wings with four different sets of design constraints. These design constraints are fixed lift distribution and net weight combined with 1) fixed maximum stress and wing loading, 2) fixed maximum deflection and wing loading, 3) fixed maximum stress and stall speed, and 4) fixed maximum deflection and stall speed. For each of these analytic solutions, the optimum wing-structure weight is found to depend only on the net weight, independent of the arbitrary fixed lift distribution. Analytic solutions for optimum weight and lift distributions are also presented for the same four sets of design constraints. Depending on the design constraints, the optimum lift distribution can differ significantly from the elliptic lift distribution. Solutions for two example wing designs are presented, which demonstrate how the induced drag varies with lift distribution, wingspan, and wing-structure weight in the design space near the optimum solution. Although the analytic solutions presented here are restricted to rectangular wings, these solutions provide excellent test cases for verifying numerical algorithms used for more general multidisciplinary analysis and optimisation.

Keywords: Lifting-line theory; Multidisciplinary design optimisation; Aerostructural optimisation; Induced-drag minimisation

Received 11 September 2019; revised 24 January 2020; accepted 19 February 2020.
This paper was originally presented at the AIAA Aviation Conference in Dallas, Texas and was published in the proceedings of that conference.

NOMENCLATURE

A	beam cross-sectional area
b	wingspan
b_δ	characteristic length associated with the deflection-limited design, Equation (55)
b_σ	characteristic length associated with the stress-limited design, Equation (38)
B_n	Fourier coefficients in the lifting-line solution for the dimensionless section-lift distribution, Equation (1)
c	local wing section chord length
c_{root}	wing section chord length at the wing root
C_{D_i}	wing induced-drag coefficient
C_L	wing lift coefficient
$C_{L_{\max}}$	wing lift coefficient at the onset of flow separation
$C_{L,\alpha}$	wing lift slope
C_δ	shape coefficient for the deflection-limited design, Equation (16)
C_σ	shape coefficient for the stress-limited design, Equation (9)
$\tilde{C}_L$	airfoil section lift coefficient
$\tilde{C}_{L_{\max}}$	airfoil section lift coefficient at the onset of flow separation
$\tilde{C}_{L,\alpha}$	airfoil section lift slope
D_i	wing induced drag
E	modulus of elasticity of the beam material
h	height of the beam cross-section
I	beam section moment of inertia
L	total wing lift
$\tilde{L}$	local wing section lift
$\tilde{M}_b$	local wing section bending moment
n_a	load factor, g
n_g	limiting load factor at the hard-landing design limit
n_m	limiting load factor at the manoeuvering-flight design limit
S	wing planform area
S_b	proportionality coefficient between $\tilde{W}_s(z)$ and $\tilde{M}_b(z)$ having units of length squared
$t_{\max}$	maximum thickness of the local airfoil section
V_∞	freestream airspeed
V_{stall}	freestream airspeed at the onset of flow separation
W	aircraft gross weight
W_n	aircraft net weight (i.e., $W–W_s$)
W_r	that portion of W_n carried at the wing root
W_s	total weight of the wing structure required to support the wing bending moment distribution
$\tilde{W}_n$	net weight of the wing per unit span (i.e., total wing weight per unit span less $\tilde{W}_s$)
$\tilde{W}_s$	weight of the wing structure per unit span required to support the wing bending moment distribution

https://doi.org/10.1017/aer.2020.24 Published online by Cambridge University Press

z spanwise coordinate relative to the midspan
γ specific weight of the beam material
δ_{max} maximum wing deflection
θ change of variables for the spanwise coordinate, Equation (1)
κ_W weight distribution coefficient, Equation (8)
ρ air density
σ_{max} maximum longitudinal stress

1.0 INTRODUCTION

For a wing with no sweep or dihedral immersed in a uniform flow, Prandtl's classical lifting-line theory[1,2] relates the section-lift distribution to the chord-length and aerodynamic-angle-of-attack distributions. Additionally, for any given wing planform, Prandtl's lifting-line theory can be used to obtain the geometric- and/or aerodynamic-twist distribution required to produce any desired section-lift distribution[3–8]. With Prandtl's lifting-line theory, an arbitrary spanwise section-lift distribution is typically written as a Fourier sine series. Although this Fourier series has been written in different forms, here we shall use the form[9]

$$\frac{b\tilde{L}(\theta)}{L} = \frac{4}{\pi}\left[\sin(\theta) + \sum_{n=2}^{\infty} B_n \sin(n\theta)\right]; \theta \equiv \cos^{-1}(-2z/b) \qquad \ldots(1)$$

The classical lifting-line solution for induced drag can be written in terms of the Fourier coefficients in Equation (1). In steady level flight, the total wing lift L must equal the gross weight W. Thus, the lifting-line solution for the induced drag in steady level flight can be written as[9]

$$D_i = \frac{2(W/b)^2}{\pi\rho V_\infty^2}\left(1 + \sum_{n=2}^{\infty} nB_n^2\right) \qquad \ldots(2)$$

For a fixed ratio of gross weight to wingspan, this induced drag is minimised with the section-lift distribution having $B_n = 0$ for all $n \geq 2$, which yields the well-known *elliptic lift distribution* introduced by Prandtl[2]. However, as pointed out by Prandtl[10], when designing a wing to minimise the induced drag in steady level flight, imposing the constraints of fixed gross weight and wingspan does not yield an absolute minimum in the induced drag.

For any given lift distribution, weight distribution, and wing structural design, there is an optimum wingspan for minimising the induced drag, which is based on the tradeoff between wingspan and wing-structure weight. Furthermore, any section-lift distribution that produces lower wing section bending moments than those produced by the elliptic lift distribution will allow the implementation of a larger wingspan for a given wing-structure weight. Because the wing-structure weight required to support the critical wing section bending moments is a function of wingspan, net weight, weight distribution, and lift distribution, designing a wing to minimise the induced drag in steady level flight requires solving a variational problem in which the weight distribution, lift distribution, wingspan, and wing-structure weight are all allowed to vary.

https://doi.org/10.1017/aer.2020.24 Published online by Cambridge University Press

The variational problem associated with designing a wing that yields an absolute minimum in induced drag was first considered by Prandtl in 1933[10]. In this paper, Prandtl obtained an analytic solution for the fixed lift distribution that minimises the induced drag under the constraints of fixed gross lift and fixed moment of inertia of gross lift, but with no constraint placed on the wingspan. Prandtl's foundational 1933 paper was originally published in German. However, a translation of that paper was recently published in English[11]. Prandtl's 1933 solution[10] for minimising induced drag under these constraints yields the dimensionless section-lift distribution[9]

$$\frac{b\tilde{L}(\theta)}{L} = \frac{4}{\pi}\left[\sin(\theta) - \frac{1}{3}\sin(3\theta)\right] \quad \ldots (3)$$

By comparison with Equation (1), Equation (3) requires $B_3 = -1/3$ and $B_n = 0$ for all $n \neq 3$. Using these Fourier coefficients in Equation (2) yields the induced drag in steady level flight for Prandtl's 1933 lift distribution, i.e.,

$$D_i = \frac{8(W/b)^2}{3\pi\rho V_\infty^2} \quad \ldots (4)$$

Comparing Equations (2) and (4), we see that Prandtl's 1933 lift distribution produces more induced drag than the elliptic lift distribution if the weight and wingspan are fixed. However, under the constraints of Prandtl's assumptions[10,11], including that the wing-structure weight is proportional to the bending moments, Prandtl's 1933 lift distribution allows a 22.5% increase in the wingspan over that allowed by the elliptic lift distribution for the same gross weight. Accounting for this wingspan increase in Equation (4), it can be shown that Prandtl's 1933 lift distribution produces 11.1% less induced drag than the elliptic lift distribution for the same gross weight[9–11]. However, it should be emphasised that Prandtl made no claim that the lift distribution in Equation (3) yields an absolute minimum in induced drag for any specific case of a physical wing[10,11]. He claimed only that this lift distribution minimises induced drag under the particular constraints of fixed gross lift and fixed moment of inertia of gross lift.

Phillips, Hunsaker, and Joo[9] have shown that Prandtl's 1933 lift distribution also yields a minimum in induced drag for the stress-limited design of a rectangular wing with fixed weight and chord-length constraints combined with the weight distribution constraint given by

$$\tilde{W}_n(z) = (W - W_r)\frac{\tilde{L}(z)}{L} - \tilde{W}_s(z) \quad \ldots (5)$$

Equation (5) alone does not completely specify the weight distribution $\tilde{W}_n(z)$. It simply provides one relation between the five design parameters, $\tilde{W}_n(z)$, W, W_r, $\tilde{W}_s(z)$, and $\tilde{L}(z)/L$. Equation (5) could be applied in the early stages of preliminary design, if no conflicting constraint is placed on the weight distribution. However, $\tilde{W}_n(z)$ cannot be evaluated from Equation (5) until the other four parameters in Equation (5) have been determined from other means.

The wing structure at each section of a wing must be sufficient to support the wing bending-moment distribution at the design limits for both manoeuvering flight and a hard landing. Because the wing bending-moment distribution depends on the weight distribution, the variational problem associated with minimising induced drag for an arbitrarily specified weight

https://doi.org/10.1017/aer.2020.24 Published online by Cambridge University Press

distribution, with no constraint placed on the wingspan, will most likely need to be solved numerically. However, the application of Equation (5) substantially reduces the constraining wing bending-moment distribution and simplifies the integration of the governing equations such that the wing-structure weight can be found analytically[9]. It has also been shown that applying Equation (5) along with the additional weight distribution constraint given by

$$W_r = \frac{n_g - 1}{n_m + n_g} W \qquad \ldots (6)$$

gives the optimum weight distribution, which minimises the bending moment required for the constraining design limit[9]. Therefore, in this paper, we will use the weight distribution described by Equations (5) and (6) to permit analytic evaluation of the wing-structure weight and to minimise the wing bending moments. As will be shown later, Equations (5) and (6) produce weight distributions that exhibit reasonable trends. However, it should be noted that the wing weight distribution is typically designed with additional constraints to those used in obtaining Equations (5) and (6). Thus, the weight distribution described by Equations (5) and (6) may not always be practical.

Using both Equations (5) and (6) yields a bending-moment distribution for the hard-landing design limit that is exactly the negative of that required for the manoeuvering-flight design limit. If W_r is larger than the value given by Equation (6), then manoeuvering flight provides the structural design limit; and if W_r is less than the value given by Equation (6), the hard landing provides the structural design limit. In any case, if the weight distribution in Equation (5) is used and the lift is positive over the entire semispan, the structural design limit for the wing bending moment can be written as[9]

$$\left|\tilde{M}_b(z)\right| = \kappa_W W_r \int_{z'=z}^{b/2} \frac{\tilde{L}(z')}{L}(z' - z)dz', \quad \text{for } z \geq 0 \qquad \ldots (7)$$

where

$$\kappa_W \equiv \begin{cases} n_m, & W_r \geq \frac{n_g - 1}{n_m + n_g} W \\ (n_g - 1)\frac{W}{W_r} - n_g, & W_r < \frac{n_g - 1}{n_m + n_g} W \end{cases} \qquad \ldots (8)$$

If the wing section bending moment is supported by any vertically symmetric beam, for a fixed maximum-stress constraint with spanwise-symmetric wing loading, the total weight of the wing structure required to support the bending-moment distribution at the design limit can be expressed as[9]

$$W_s = 2 \int_{z=0}^{b/2} \frac{|\tilde{M}_b(z)|}{S_b(z)} dz; \quad S_b(z) \equiv \frac{C_\sigma (t_{\max}/c) c(z) \sigma_{\max}}{\gamma}, \quad C_\sigma \equiv \frac{2I(h/t_{\max})}{Ah^2} \qquad \ldots (9)$$

Equations for computing values of C_σ for some common beam cross-sections are presented in Ref. (9).

We see from Equation (9) that, for any spanwise-symmetric wing loading, the weight of the wing structure required to support a maximum-stress constraint is proportional to the integral

https://doi.org/10.1017/aer.2020.24 Published online by Cambridge University Press

of the bending-moment distribution divided by the chord-length distribution. Because, in the development of his 1933 lift distribution, Prandtl assumed a proportionality coefficient between $\tilde{M}_b$ and $\tilde{W}_s$ that is independent of z[10], the resulting minimum-drag analysis may not apply to the stress-limited design of a wing with a chord length and thickness that vary with the spanwise coordinate. However, Prandtl's 1933 minimum-drag analysis could be applied to the stress-limited design of a rectangular wing with the weight distribution specified by Equation (5).

Approaches similar to that of Prandtl have been taken by others to find analytic solutions to this complex, variational, optimisation problem. For example, Jones[12] looked at minimising the induced drag for a given lift and root bending moment. Later, Jones and Lasinski[13] added a constraint on the integrated bending moment and included the effects of winglets. Klein and Viswanathan have also considered the problem of a given total lift and root bending moment[14] and have extended the theory to include a given wing-structure weight[15]. More recently, Phillips, Hunsaker, and Joo[9] have presented both stress-limited and deflection-limited solutions for minimising induced drag on a rectangular wing with fixed weight and wing-loading constraints. The work of Phillips, Hunsaker, and Joo[9] has also been extended to account for the effects of wing taper by Taylor and Hunsaker[16]. Other relevant publications include[17–28].

Combining Equations (1), (7), and (9), Phillips, Hunsaker, and Joo[9] have shown that, for the stress-limited design of a rectangular wing with any all-positive spanwise-symmetric lift distribution and the weight distribution specified by Equation (5), the required weight of the wing structure is given by[9]

$$W_s = \frac{\kappa_W W_r b^2}{32 S_b}(1 + B_3) \qquad \ldots (10)$$

Notice from Equation (2) that all Fourier coefficients B_n make a positive contribution to the induced drag. However, we see from Equation (10) that only B_3 contributes to the required structure weight of a rectangular wing with any all-positive spanwise-symmetric lift distribution and the weight distribution specified by Equation (5).

For the *stress-limited design* of a rectangular wing with the weight distribution specified by Equation (5) and any all-positive spanwise-symmetric lift distribution, the total weight of the wing structure required to support the bending-moment distribution at the design limit is given by[9]

$$W_s = \frac{\gamma (W/S)}{32 C_\sigma (t_{\max}/c)\sigma_{\max}} \frac{\kappa_W W_r b^3}{W}(1 + B_3) \qquad \ldots (11)$$

Under the constraints of *a fixed lift distribution, fixed gross weight, fixed maximum stress, and fixed wing loading*, the induced drag on a rectangular wing is minimised using a lift distribution having

$$B_3 = -3/8 + \sqrt{9/64 - 1/12}; \quad B_n = 0, \text{ for } n \neq 3 \qquad \ldots (12)$$

which yields the optimum results

$$\frac{b\tilde{L}(\theta)}{L} = \frac{4}{\pi}[\sin(\theta) - 0.13564322 \ \sin(3\theta)] \qquad \ldots (13)$$

https://doi.org/10.1017/aer.2020.24 Published online by Cambridge University Press

$$b = \sqrt[3]{\frac{32C_\sigma(t_{\max}/c)\sigma_{\max}}{0.86435678\,\gamma(W/S)}\frac{W_s W}{\kappa_W W_r}} \quad \ldots(14)$$

$$D_i = \frac{2.11039450}{\pi\rho V_\infty^2}\left[\frac{0.86435678\,\gamma(W/S)}{32C_\sigma(t_{\max}/c)\sigma_{\max}}\frac{\kappa_W W_r W^2}{W_s}\right]^{2/3} \quad \ldots(15)$$

Taylor and Hunsaker[16] have also shown that for linearly tapered wings, the lift distribution that minimises induced drag is very similar to that shown in Equation (13), regardless of the degree of taper.

For the *deflection-limited design* of a rectangular wing with the weight distribution specified by Equation (5) and any all-positive spanwise-symmetric lift distribution, the total weight of the wing structure required to support the bending-moment distribution at the design limit is given by[9]

$$W_s = \frac{\gamma(W/S)^2}{32C_\delta E(t_{\max}/c)^2\delta_{\max}}\frac{\kappa_W W_r b^6}{W^2}(1+B_3); \quad C_\delta \equiv \frac{8I(h/t_{\max})^2}{Ah^2} \quad \ldots(16)$$

Under the constraints of *a fixed lift distribution, fixed gross weight, fixed maximum deflection, and fixed wing loading*, the induced drag is minimised using a lift distribution having

$$B_3 = -3/7 + \sqrt{9/49 - 1/21}; \quad B_n = 0, \text{ for } n \neq 3 \quad \ldots(17)$$

which yields the optimum results

$$\frac{b\tilde{L}(\theta)}{L} = \frac{4}{\pi}[\sin(\theta) - 0.05971587\ \sin(3\theta)] \quad \ldots(18)$$

$$b = \sqrt[6]{\frac{32C_\delta E(t_{\max}/c)^2\delta_{\max}}{0.94028413\,\gamma(W/S)^2}\frac{W_s W^2}{\kappa_W W_r}} \quad \ldots(19)$$

$$D_i = \frac{2.02139591}{\pi\rho V_\infty^2}\left[\frac{0.94028413\,\gamma(W/S)^2}{32C_\delta E(t_{\max}/c)^2\delta_{\max}}\frac{\kappa_W W_r W^4}{W_s}\right]^{1/3} \quad \ldots(20)$$

Note that although deflection limits may not always be explicitly enforced in practice, some limit on deflection should at least be considered to preclude wing strike during a hard landing. Furthermore, excessive wingtip deflection during flight can adversely affect the aerodynamics and flight mechanics of an aircraft. For highly flexible aircraft, these adverse effects can be very significant[29]. Therefore, in this paper, both stress and deflection limits will be considered.

The optimum lift distributions given in Equations (3), (13), and (18) were all obtained under the constraint that a single lift distribution is used during all flight phases, and the same constraint is used for all subsequent results presented in this paper. However, in general, the lift distribution for a wing with fixed geometry changes depending on the load factor. Therefore,

https://doi.org/10.1017/aer.2020.24 Published online by Cambridge University Press

in order for this constraint to be satisfied, we must assume that wing twist can be varied during flight to maintain a single lift distribution at all loading conditions. This can be done using variable geometric and/or aerodynamic twist[30–35]. However, the designer is not always constrained to a single lift distribution. Variable geometric and/or aerodynamic twist can also be used to implement different lift distributions during different flight phases[4,5,7,8,30–35]. For example, the lift distribution given by Equation (13) could be implemented during high-load-factor manoeuvers; other lift distributions could be implemented during takeoff and landing; and the elliptic lift distribution could be implemented during steady level flight. This would allow an increase in the wingspan over that allowed by a fixed elliptic lift distribution, without increasing the gross weight or imposing any induced-drag penalty during steady level flight.

Although the approximations associated with lifting-line theory were used to obtain the solutions presented here, for unswept wings of aspect ratio greater than 4, lifting-line theory has been shown to be in excellent agreement with experimental data and grid-resolved CFD solutions, and lifting-line solutions are widely accepted[3–7,36–71]. Furthermore, although some important design considerations are neglected when using lifting-line theory, analytic solutions such as those presented in this paper provide insight into the relationships between design parameters and the relative influence of those parameters on the aerodynamics of a finite wing. In fact, a significant portion of our current understanding of finite-wing aerodynamics, including the relationship between lift distribution, twist distribution, chord distribution, and induced drag, comes from early analytic solutions based on lifting-line theory. Designers often rely on principles based on these solutions during conceptual design phases. Some of these solutions are also used for benchmarking numerical tools. The results presented in this paper have the same utility as these early analytic solutions. As will be shown, the results in this paper reveal important aspects about the aerodynamic and structural coupling involved in designing a wing for minimum induced drag and provide excellent examples for benchmarking higher-fidelity multidisciplinary optimisation tools.

2.0 MINIMISING INDUCED DRAG WITH WINGSPAN AND WING-STRUCTURE WEIGHT

Minimising induced drag by varying the wingspan and lift distribution while holding gross weight constant is not the only variational problem suggested by Equation (2). Because the wing-structure weight is proportional to the wing bending moments, the wing-structure weight increases with increasing wingspan for any fixed lift and weight distributions. Therefore, Equation (2) also suggests that the induced drag could be minimised by varying the wingspan b and allowing the wing-structure weight W_s to change while holding the net weight W_n and lift distribution $b\tilde{L}(z)/L$ fixed. Because the required wing-structure weight depends on both the wingspan and the lift distribution, in general, W_s depends on b and all of the Fourier coefficients B_n. Because gross weight is simply the sum of W_n and W_s, for an arbitrary wing design, Equation (2) can be written

$$D_i = \frac{2}{\pi\rho V_\infty^2}\left(\frac{W_n}{b} + \frac{W_s(b, B_n)}{b}\right)^2 \left(1 + \sum_{n=2}^{\infty} nB_n^2\right) \qquad \ldots(21)$$

For any fixed W_n, the term W_n/b always decreases with increasing wingspan; and for typical design constraints, the term $W_s(b, B_n)/b$ increases with increasing wingspan. For example, the design constraints that led to Prandtl's 1933 lift distribution yield W_s proportional to b^2 as

https://doi.org/10.1017/aer.2020.24 Published online by Cambridge University Press

given in Equation (10); the design constraints that led to the lift distribution given in Equation (13) yield W_s proportional to b^3 as given in Equation (11); and the design constraints that led to the lift distribution given in Equation (18) yield W_s proportional to b^6 as given in Equation (16). For any fixed lift and weight distributions, there is an optimum wingspan for minimising the induced drag, which is based on the tradeoff between the wingspan b and the wing-structure weight W_s.

For example, for the stress-limited design of a rectangular wing with the weight distribution specified by Equation (5) and any all-positive spanwise-symmetric lift distribution, the total weight of the wing structure required to support the bending-moment distribution at the design limit is given by Equation (11). The gross weight is the sum $W = W_n + W_s$. Hence, using Equation (11) in Equation (21), the induced drag can be written as

$$D_i = \frac{2}{\pi\rho V_\infty^2}\left[\frac{W_n}{b} + \frac{(1+B_3)\gamma(W/S)}{32C_\sigma(t_{\max}/c)\sigma_{\max}}\frac{\kappa_W W_r b^2}{W}\right]^2\left(1+\sum_{n=2}^{\infty} nB_n^2\right) \quad \ldots(22)$$

For any given value of the ratio $\kappa_W W_r/W$, the function in the square brackets of Equation (22) can be minimised with respect to b, based on the tradeoff between wingspan and wing-structure weight.

To minimise the ratio $\kappa_W W_r/W$ for any given wingspan, the weight distribution given by Equation (6) can be used. Hence, using Equation (6) in Equations (8) and (11) yields $\kappa_W = n_m$ and

$$W_s = \frac{(1+B_3)\gamma(W/S)}{32C_\sigma(t_{\max}/c)\sigma_{\max}}\frac{n_m(n_g-1)}{n_m+n_g}b^3 \quad \ldots(23)$$

From Equations (6), (8), and (22) the induced drag is

$$D_i = \frac{2}{\pi\rho V_\infty^2}\left[\frac{W_n}{b} + \frac{(1+B_3)\gamma(W/S)}{32C_\sigma(t_{\max}/c)\sigma_{\max}}\frac{n_m(n_g-1)}{n_m+n_g}b^2\right]^2\left(1+\sum_{n=2}^{\infty} nB_n^2\right) \quad \ldots(24)$$

The wingspan that minimises this induced drag for a fixed lift distribution and fixed wing loading is

$$b = \sqrt[3]{\frac{16C_\sigma(t_{\max}/c)\sigma_{\max}W_n}{(1+B_3)\gamma(W/S)}\frac{n_m+n_g}{n_m(n_g-1)}} \quad \ldots(25)$$

Using Equation (25) in Equation (23), the wing-structure weight that minimises this induced drag for any fixed value of B_3 is

$$W_s = \frac{1}{2}W_n \quad \ldots(26)$$

Using Equation (25) in Equation (24), the associated minimum induced drag is

$$D_i = \frac{9}{2\pi\rho V_\infty^2}\left[\frac{(1+B_3)\gamma(W/S)W_n^2}{16C_\sigma(t_{\max}/c)\sigma_{\max}}\frac{n_m(n_g-1)}{n_m+n_g}\right]^{2/3}\left(1+\sum_{n=2}^{\infty} nB_n^2\right) \quad \ldots(27)$$

https://doi.org/10.1017/aer.2020.24 Published online by Cambridge University Press

It should be emphasised that the wing-structure weight is not an independent variable, but rather a dependent variable, related to the wingspan, lift distribution, load factor, and other independent design variables, as shown in Equation (23). Therefore, the relation shown in Equation (26) results from the optimum solution, and requires that the optimum net weight distribution and wingspan are used in accordance with the design constraints.

Equation (27) gives the minimum possible induced drag for the stress-limited design of a rectangular wing with fixed wing loading, the weight distribution specified by Equation (5), and any fixed all-positive spanwise-symmetric lift distribution. However, even though Equation (6) was used to minimise the ratio $\kappa_W W_r / W$ in Equation (22), Equation (27) does not provide an absolute minimum in induced drag for the specified design constraints and weight distribution, unless the optimum lift distribution is also used. From Equation (27), we see that the variation of this drag with the Fourier coefficients B_n is proportional to $(1 + \Sigma n B_n^2)(1 + B_3)^{2/3}$. Minimising this function yields the Fourier coefficients given in Equation (12) and the optimum lift distribution given in Equation (13).

The optimum wing-structure weight given in Equation (26) and the optimum lift distribution given in Equation (13) are for the stress-limited design of a rectangular wing with fixed wing loading. However, Taylor and Hunsaker[16] have shown that the solution given in Equation (26) also holds for the stress-limited design of a tapered wing with fixed wing loading. Furthermore, the reader is reminded that the optimum lift distribution that minimises induced drag for tapered wings does not deviate significantly from that given in Equation (13), regardless of the degree of taper[16].

For the deflection-limited design of a rectangular wing with any fixed all-positive spanwise-symmetric lift distribution and the weight distribution specified by Equations (5) and (6), the total weight of the wing structure required to support the bending-moment distribution at the design limit is given by Equation (16). Hence, using Equations (6), (8), and (16) with the relation $W = W_n + W_s$ yields

$$W = W_n + \frac{(1 + B_3)\gamma (W/S)^2}{32 C_\delta E (t_{\max}/c)^2 \delta_{\max}} \frac{n_m (n_g - 1)}{n_m + n_g} \frac{b^6}{W} \qquad \ldots (28)$$

Equation (28) is easily solved for the gross weight, and using the relation $W_s = W - W_n$ yields

$$W_s = -\frac{W_n}{2} + \sqrt{\frac{W_n^2}{4} + \frac{(1 + B_3)\gamma (W/S)^2}{32 C_\delta E (t_{\max}/c)^2 \delta_{\max}} \frac{n_m (n_g - 1)}{n_m + n_g} b^6} \qquad \ldots (29)$$

Using this wing-structure weight with the relation $W = W_n + W_s$ in Equation (2) gives

$$D_i = \frac{2}{\pi \rho V_\infty^2} \left(\frac{W_n}{2b} + \sqrt{\frac{W_n^2}{4b^2} + \frac{(1 + B_3)\gamma (W/S)^2}{32 C_\delta E (t_{\max}/c)^2 \delta_{\max}} \frac{n_m (n_g - 1)}{n_m + n_g} b^4} \right)^2 \left(1 + \sum_{n=2}^{\infty} n B_n^2 \right) \qquad \ldots (30)$$

The wingspan that minimises this induced drag for any fixed W_n, fixed lift distribution, and fixed wing loading is

https://doi.org/10.1017/aer.2020.24 Published online by Cambridge University Press

$$b = \sqrt[6]{\frac{10C_\delta E(t_{\max}/c)^2 \delta_{\max} W_n^2}{(1+B_3)\gamma(W/S)^2} \frac{n_m + n_g}{n_m(n_g - 1)}} \quad \ldots(31)$$

Using Equation (31) in Equation (29), the wing-structure weight that minimises this induced drag for any fixed value of B_3 is

$$W_s = \frac{1}{4} W_n \quad \ldots(32)$$

Using Equation (31) in Equation (30), the associated minimum induced drag is

$$D_i = \frac{25}{8\pi\rho V_\infty^2} \left[\frac{(1+B_3)\gamma(W/S)^2 W_n^4}{10C_\delta E(t_{\max}/c)^2 \delta_{\max}} \frac{n_m(n_g-1)}{n_m+n_g} \right]^{1/3} \left(1 + \sum_{n=2}^{\infty} n B_n^2 \right) \quad \ldots(33)$$

Here again, even though Equation (6) was used to minimise W_s for any given wingspan, Equation (33) does not provide an absolute minimum in induced drag for the specified design constraints and weight distribution, unless the optimum lift distribution is also used. From Equation (33), we see that the variation of this drag with the Fourier coefficients B_n is proportional to $(1 + \Sigma n B_n^2)(1 + B_3)^{1/3}$. Minimising this function yields the Fourier coefficients given in Equation (17) and the optimum lift distribution given in Equation (18).

The optimum wing-structure weights shown in Equations (26) and (32) are typical of those seen in many sailplanes[72]. This should not be surprising, since sailplanes are designed to operate with maximum efficiency at conditions where induced drag is a significant portion of the total drag. However, for other aircraft types, these results may not be practical due to additional constraints. Moreover, the results shown in Equations (23)–(27) and (29)–(33) are for a rectangular wing with the weight distribution given in Equations (5) and (6), which minimises the bending moment required for any given wingspan at the constraining design limit. However, the reader is reminded that this weight distribution is not always practical due to other design constraints. Numerical methods can be used to evaluate the optimum wingspan and wing-structure weight required to minimise induced drag for other weight distributions and/or wing planforms[16].

3.0 MINIMUM INDUCED DRAG FOR FIXED NET WEIGHT, MAXIMUM STRESS, AND STALL SPEED

Minimising induced drag for a rectangular wing with spanwise-symmetric lift and the weight distribution specified by Equation (5) requires a lift distribution having $B_n = 0$ for all $n \neq 3$ with $-1/3 \leq B_3 \leq 0$. Using these constraints in Equation (1) yields

$$\tilde{C}_L(\theta) = \frac{4}{\pi} C_L[\sin(\theta) + B_3 \sin(3\theta)] \quad \ldots(34)$$

For a rectangular wing with $-1/3 \leq B_3 \leq 0$, the maximum section lift coefficient always occurs at the wing root, i.e., $\theta = \pi/2$. From Equation (34), the maximum wing lift coefficient is related to the maximum section lift coefficient by

https://doi.org/10.1017/aer.2020.24 Published online by Cambridge University Press

$$C_{L_{\max}} = \frac{\pi}{4[\sin(\pi/2) + B_3 \sin(3\pi/2)]}\tilde{C}_{L_{\max}} = \frac{\pi}{4(1-B_3)}\tilde{C}_{L_{\max}} \qquad \ldots(35)$$

At the stall speed, Equation (35) requires

$$\frac{n_a(W_n + W_s)}{\frac{1}{2}\rho V_{\text{stall}}^2 S} = \frac{\pi}{4(1-B_3)}\tilde{C}_{L_{\max}} \text{ or } S = \frac{8(1-B_3)n_a(W_n+W_s)}{\pi\,\rho V_{\text{stall}}^2 \tilde{C}_{L_{\max}}} \qquad \ldots(36)$$

For the stress-limited design of a rectangular wing with any fixed all-positive spanwise-symmetric lift distribution and the weight distribution specified by Equation (5), the total weight of the wing structure required to support the bending-moment distribution at the design limit is given by Equation (11). To minimise the ratio $\kappa_W W_r/W$ for any given wingspan, the optimum weight distribution given in Equation (6) can be used as well. Thus, using Equations (6) and (8) in Equation (11) and rearranging yields

$$W_s = \frac{\gamma\, n_m(n_g-1)(W_n+W_s)}{32C_\sigma(t_{\max}/c)\sigma_{\max}(n_m+n_g)}\frac{(1+B_3)b^3}{S} \qquad \ldots(37)$$

At this point it is convenient to define an important characteristic length associated with this stress-limited design

$$b_\sigma \equiv \left[\frac{C_\sigma(t_{\max}/c)\sigma_{\max}n_a(n_m+n_g)W_n}{\pi\,\rho V_{\text{stall}}^2\tilde{C}_{L_{\max}}\gamma\, n_m(n_g-1)}\right]^{1/3} \qquad \ldots(38)$$

Using Equations (36) and (38) to eliminate the planform area from Equation (37) yields

$$W_s = \frac{(1+B_3)W_n b^3}{256(1-B_3)b_\sigma^3} \qquad \ldots(39)$$

Using this wing-structure weight with the relation $W = W_n + W_s$ in Equation (2) gives

$$D_i = \frac{2}{\pi\rho V_\infty^2}\left[\frac{W_n}{b} + \frac{(1+B_3)W_n b^2}{256(1-B_3)b_\sigma^3}\right]^2\left(1+\sum_{n=2}^{\infty} nB_n^2\right) \qquad \ldots(40)$$

The wingspan that minimises this induced drag for any fixed lift distribution and net weight is

$$b = \left(\frac{128(1-B_3)}{1+B_3}\right)^{1/3} b_\sigma \qquad \ldots(41)$$

Using Equation (41) to eliminate b from Equation (39), the wing-structure weight that minimises the induced drag for fixed W_n, fixed $\sigma_{\max}$, fixed V_{stall}, and any fixed value of B_3 is

$$W_s = \frac{1}{2}W_n \qquad \ldots(42)$$

https://doi.org/10.1017/aer.2020.24 Published online by Cambridge University Press

Using Equation (41) to eliminate b from Equation (40) with $B_n = 0$ for all $n \neq 3$, the minimum induced drag for a fixed lift distribution, fixed W_n, fixed $\sigma_{\max}$, and fixed V_{stall} can be written as

$$D_i = \left(\frac{1+B_3}{128(1-B_3)}\right)^{2/3} \frac{9(1+3B_3^2)W_n^2}{2\pi\rho V_\infty^2 b_\sigma^2} \quad \ldots (43)$$

The variation of this drag with B_3 is proportional to $[(1+3B_3^2)^3(1+B_3)^2/(1-B_3)^2]^{1/3}$. Thus, for fixed W_n, fixed $\sigma_{\max}$, and fixed V_{stall}, the value of B_3 that minimises the induced drag predicted from Equation (43) is obtained from

$$9B_3^3 - 6B_3^2 - 9B_3 - 2 = 0 \quad \ldots (44)$$

The roots of this cubic equation are

$$B_3 = \frac{1}{2} - \sqrt{\frac{11}{12}}, \quad B_3 = -\frac{1}{3}, \quad B_3 = \frac{1}{2} + \sqrt{\frac{11}{12}} \quad \ldots (45)$$

Using the only root in the range $-1/3 \leq B_3 \leq 0$, Equations (1), (41), (36), and (43) result in

$$\frac{b\tilde{L}(\theta)}{L} = \frac{4}{\pi}[\sin(\theta) - \frac{1}{3}\sin(3\theta)] \quad \ldots (46)$$

$$b = \sqrt[3]{256}\, b_\sigma \quad \ldots (47)$$

$$S = \frac{16 n_a W_n}{\pi\, \rho V_{\text{stall}}^2 \tilde{C}_{L_{\max}}} \quad \ldots (48)$$

$$D_i = \frac{6W_n^2}{(256^{2/3})\pi\rho V_\infty^2 b_\sigma^2} \quad \ldots (49)$$

For a fixed elliptic lift distribution, Equations (41), (36), and (43) result in

$$b = \sqrt[3]{128}\, b_\sigma \quad \ldots (50)$$

$$S = \frac{12 n_a W_n}{\pi\, \rho V_{\text{stall}}^2 \tilde{C}_{L_{\max}}} \quad \ldots (51)$$

$$D_i = \frac{9W_n^2}{2(128^{2/3})\pi\rho V_\infty^2 b_\sigma^2} \quad \ldots (52)$$

In summary, under the constraints of *a fixed lift distribution, fixed net weight, fixed maximum stress, and fixed stall speed*, minimising induced drag for a rectangular wing with spanwise-symmetric lift and the optimum weight distribution specified by Equations (5) and (6) requires a lift distribution having $B_n = 0$ for all $n \neq 3$ with $-1/3 \leq B_3 \leq 0$. With these constraints and any fixed value of B_3, the induced drag is minimised using a wing-structure weight

https://doi.org/10.1017/aer.2020.24 Published online by Cambridge University Press

equal to one half the net weight as given in Equation (42). This induced drag is further minimised by using the lift distribution given in Equation (46), which is exactly Prandtl's 1933 lift distribution as given in Equation (3). Comparing Equations (47)–(49) with Equations (50)–(52), we see that, for this wing geometry, weight distribution, and design constraints, the fixed lift distribution given in Equation (46) results in a 25.99% increase in the wingspan, a 33.33% increase in the planform area, and a 16.01% decrease in the induced drag over those obtained for a fixed elliptic lift distribution with the same net weight, maximum stress, and stall speed.

4.0 MINIMUM INDUCED DRAG FOR FIXED NET WEIGHT, MAXIMUM DEFLECTION, AND STALL SPEED

For the deflection-limited design of a rectangular wing with any fixed all-positive spanwise-symmetric lift distribution and the weight distribution specified by Equation (5), the total weight of the wing structure required to support the bending-moment distribution at the design limit is given by Equation (16), which can be rearranged as

$$W_s = \frac{\gamma \kappa_W W_r}{32 C_\delta E (t_{\max}/c)^2 \delta_{\max}} \frac{(1+B_3) b^6}{S^2} \qquad \ldots (53)$$

Using Equation (36) to eliminate the planform area from Equation (53) and applying Equation (6) to minimise W_s for any given wingspan yields

$$W_s = \frac{(1+B_3) b^6 W_n^2}{2048\,(1-B_3)^2 b_\delta^6 (W_n + W_s)} \qquad \ldots (54)$$

where b_δ is an important characteristic length associated with this deflection-limited design,

$$b_\delta \equiv \left[\frac{C_\delta E (t_{\max}/c)^2 \delta_{\max} n_a^2 (n_m + n_g) W_n^2}{(\pi \rho V_{\text{stall}}^2 \tilde{C}_{L_{\max}})^2 \gamma n_m (n_g - 1)} \right]^{1/6} \qquad \ldots (55)$$

Equation (54) can be rearranged as a quadratic equation in W_s to give

$$W_s^2 + W_n W_s - \frac{(1+B_3) b^6 W_n^2}{2048\,(1-B_3)^2 b_\delta^6} = 0 \qquad \ldots (56)$$

The only positive root of Equation (56) is given by

$$W_s = -\frac{W_n}{2} + \frac{W_n}{2} \sqrt{1 + \frac{(1+B_3) b^6}{512\,(1-B_3)^2 b_\delta^6}} \qquad \ldots (57)$$

Using this wing-structure weight with the relation $W = W_n + W_s$ in Equation (2) gives

$$D_i = \frac{2}{\pi \rho V_\infty^2} \left[\frac{W_n}{2} \left(\frac{1}{b} + \sqrt{\frac{1}{b^2} + \frac{(1+B_3) b^4}{512\,(1-B_3)^2 b_\delta^6}} \right) \right]^2 \left(1 + \sum_{n=2}^{\infty} n B_n^2 \right) \qquad \ldots (58)$$

https://doi.org/10.1017/aer.2020.24 Published online by Cambridge University Press

The wingspan that minimises this induced drag for any fixed lift distribution and net weight is

$$b = \left[\frac{640(1-B_3)^2}{(1+B_3)}\right]^{1/6} b_\delta \quad \ldots(59)$$

Using Equation (59) to eliminate b from Equation (57), the wing-structure weight that minimises the induced drag for fixed W_n, fixed δ_{max}, fixed V_{stall}, and any fixed value of B_3 is

$$W_s = \frac{1}{4} W_n \quad \ldots(60)$$

Using Equation (59) to eliminate b from Equation (58) with $B_n = 0$ for all $n \neq 3$, the minimum induced drag for a fixed lift distribution, fixed W_n, fixed δ_{max}, and fixed V_{stall} can be written as

$$D_i = \left(\frac{1+B_3}{10(1-B_3)^2}\right)^{1/3} \frac{25(1+3B_3^2)W_n^2}{32\pi\rho V_\infty^2 b_\delta^2} \quad \ldots(61)$$

The variation of this drag with B_3 is proportional to $[(1+3B_3^2)^3(1+B_3)/(1-B_3)^2]^{1/3}$. Thus, for fixed W_n, fixed δ_{max}, and fixed V_{stall}, the value of B_3 that minimises the induced drag predicted from Equation (61) is obtained from

$$15B_3^3 - 9B_3^2 - 19B_3 - 3 = 0 \quad \ldots(62)$$

The roots of this cubic equation are

$$B_3 = -0.74279033, B_3 = -0.17714856, B_3 = 1.5199389 \quad \ldots(63)$$

Using the only root in the range $-1/3 \leq B_3 \leq 0$, Equations (1), (59), (36), and (61) result in

$$\frac{b\tilde{L}(\theta)}{L} = \frac{4}{\pi}[\sin(\theta) - 0.17714856\sin(3\theta)] \quad \ldots(64)$$

$$b = 3.2019916\, b_\delta \quad \ldots(65)$$

$$S = 11.771486 \frac{n_a W_n}{\pi\, \rho V_{stall}^2 \tilde{C}_{L_{max}}} \quad \ldots(66)$$

$$D_i = 0.33349127 \frac{W_n^2}{\pi\rho V_\infty^2 b_\delta^2} \quad \ldots(67)$$

For a fixed elliptic lift distribution, Equations (59), (36), and (61) result in

$$b = (640^{1/6}) b_\delta \quad \ldots(68)$$

https://doi.org/10.1017/aer.2020.24 Published online by Cambridge University Press

$$S = \frac{10 n_a W_n}{\pi \rho V_{\text{stall}}^2 \tilde{C}_{L_{\max}}} \quad \ldots (69)$$

$$D_i = \frac{25 W_n^2}{32(10^{1/3})\pi \rho V_\infty^2 b_\delta^2} \quad \ldots (70)$$

In summary, under the constraints of *a fixed lift distribution, fixed net weight, fixed maximum deflection, and fixed stall speed*, minimising induced drag for a rectangular wing with spanwise-symmetric lift and the optimum weight distribution specified by Equations (5) and (6) requires a lift distribution having $B_n = 0$ for all $n \neq 3$ and $-1/3 \leq B_3 \leq 0$. With these constraints and any fixed value of B_3, induced drag is minimised using a wing-structure weight equal to one fourth the net weight as given in Equation (60). This induced drag is further minimised by using the lift distribution given in Equation (64). Comparing Equations (65)–(67) with Equations (68)–(70), we see that, for this wing geometry, weight distribution, and design constraints, the fixed lift distribution given in Equation (64) results in a 9.07% increase in the wingspan, a 17.71% increase in the planform area, and an 8.03% decrease in the induced drag over those obtained for a fixed elliptic lift distribution with the same net weight, maximum deflection, and stall speed.

It should be noted that for both the stress-limited design and the deflection-limited design of a rectangular wing with fixed stall speed, the optimum solution requires an increase in planform area over a wing designed with a fixed elliptic lift distribution. Because the viscous drag is related to the planform area, the designs that minimise induced drag may not be the designs that minimise total drag. The same is true for the case of fixed wing loading, where a change in wing-structure weight requires a corresponding change in the wing area. Moreover, in order to obtain the optimum lift distributions given in Equations (13), (18), (46) and (64) on a rectangular planform, the wing must be twisted. As shown by Stewart and Hunsaker[73], the viscous drag introduced by this twist can reduce the benefits of using the minimum-induced-drag solution. Therefore, when designing a wing for minimum total drag, viscous effects should be considered. Although viscous effects are not considered in this study, the optimum solutions presented here provide valuable insight into the coupling between lift distribution, wingspan, and wing-structure weight and their effect on induced drag.

5.0 RESULTS

The optimum wingspans given in Equations (25), (31), (41), and (59) all minimise induced drag for a rectangular wing with fixed net weight and any fixed all-positive spanwise-symmetric lift distribution combined with other design constraints. Equation (25) is for a stress-limited design with fixed wing loading; Equation (31) is for a deflection-limited design with fixed wing loading; Equation (41) is for a stress-limited design with fixed stall speed; and Equation (59) is for a deflection-limited design with fixed stall speed. The optimum wing-structure weights corresponding to the optimum wingspans given in Equations (25), (31), (41), and (59) are respectively given in Equations (26), (32), (42), and (60). Although induced drag depends on all of the Fourier coefficients B_n in Equation (1), for an arbitrary lift distribution, the optimum wingspans computed from Equations (25), (31), (41), and (59) depend only on the single Fourier coefficient B_3.

Although the wingspans from Equations (25), (31), (41), and (59) give the minimum possible induced drag for the specified design constraints and any fixed all-positive

https://doi.org/10.1017/aer.2020.24 Published online by Cambridge University Press

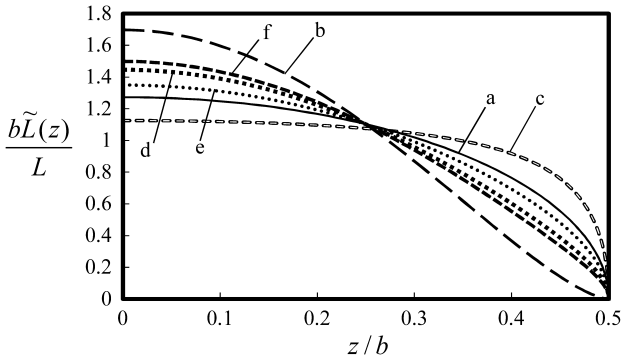

Figure 1. Lift distributions from Equations (13), (18), (46), and (64) compared with the elliptic distribution and that for an untwisted rectangular wing of aspect ratio 8.

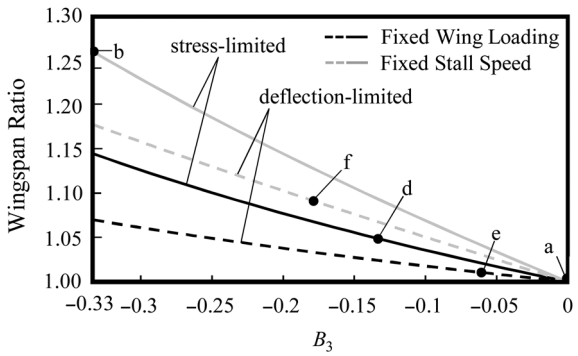

Figure 2. Ratio of the optimum wingspan, as a function of B_3, to the optimum wingspan for the fixed elliptic lift distribution for the stress- and deflection-limited design of a wing with fixed wing loading or fixed stall speed.

spanwise-symmetric lift distribution, these optimum wingspans do not provide an absolute minimum in induced drag for the specified design constraints unless the optimum lift distribution is also used. The optimum lift distributions corresponding to the optimum wingspans given in Equations (25), (31), (41), and (59) are respectively given in Equations (13), (18), (46), and (64). Figure 1 shows each of these four lift distributions compared with the elliptic lift distribution and the lift distribution produced by an untwisted rectangular wing. The distribution labeled (a) is the elliptic lift distribution, and that labeled (b) is Prandtl's 1933 lift distribution, which is also the lift distribution given in Equation (46) that minimises induced drag for a stress-limited design with fixed stall speed. The lift distribution labeled (c) is that produced by an untwisted rectangular wing of aspect ratio 8. Lift distribution (d) is that from Equation (13), which minimises induced drag for a stress-limited design with fixed wing loading, (e) is the lift distribution from Equation (18) that minimises induced drag for a deflection-limited design with fixed wing loading, and (f) is the lift distribution from Equation (64) that minimises induced drag for a deflection-limited design with fixed stall speed.

For any given lift distribution, the wingspan that minimises induced drag depends on B_3 and the design constraints. For each of the design constraints considered in this paper, the nature of this dependence can be seen in Fig. 2, which shows the ratio of the optimum wingspan for any

https://doi.org/10.1017/aer.2020.24 Published online by Cambridge University Press

given value of B_3 in the range $-1/3 \le B_3 \le 0$ to the optimum wingspan for the fixed elliptic lift distribution with the same set of design constraints. The wingspan ratios corresponding to the optimum lift distributions (a), (b), (d), (e), and (f) from Fig. 1 are labeled in Fig. 2 for reference.

For any acceptable design, both the stress and deflection constraints must be satisfied. For the stress-limited design with fixed wing loading, combining Equations (23) and (2) yields the following relations for the wingspan and induced drag expressed as a function of the wing-structure weight

$$b = \left[\frac{32C_\sigma(t_{\max}/c)\sigma_{\max}}{(1+B_3)\gamma(W/S)}\frac{n_m+n_g}{n_m(n_g-1)}W_s\right]^{1/3} \quad \ldots(71)$$

$$D_i = \frac{2}{\pi\rho V_\infty^2}\left[\frac{(1+B_3)\gamma(W/S)}{32C_\sigma(t_{\max}/c)\sigma_{\max}}\frac{n_m(n_g-1)}{n_m+n_g}\frac{(W_n+W_s)^3}{W_s}\right]^{2/3}\left(1+\sum_{n=2}^{\infty}nB_n^2\right) \quad \ldots(72)$$

Similarly, for the deflection-limited design with fixed wing loading, combining Equations (29) and (2) results in

$$b = \left[\frac{32C_\delta E(t_{\max}/c)^2\delta_{\max}}{(1+B_3)\gamma(W/S)^2}\frac{n_m+n_g}{n_m(n_g-1)}W_s(W_n+W_s)\right]^{1/6} \quad \ldots(73)$$

$$D_i = \frac{2}{\pi\rho V_\infty^2}\left[\frac{(1+B_3)\gamma(W/S)^2}{32C_\delta E(t_{\max}/c)^2\delta_{\max}}\frac{n_m(n_g-1)}{n_m+n_g}\frac{(W_n+W_s)^5}{W_s}\right]^{1/3}\left(1+\sum_{n=2}^{\infty}nB_n^2\right) \quad \ldots(74)$$

For the stress-limited design with fixed stall speed, combining Equations (39) and (2) yields

$$b = \left[\frac{256(1-B_3)W_s}{(1+B_3)W_n}\right]^{1/3} b_\sigma \quad \ldots(75)$$

$$D_i = \frac{2}{\pi\rho V_\infty^2}\left[\frac{(1+B_3)W_n(W_n+W_s)^3}{256(1-B_3)W_s b_\sigma^3}\right]^{2/3}\left(1+\sum_{n=2}^{\infty}nB_n^2\right) \quad \ldots(76)$$

and for the deflection-limited design with fixed stall speed, combining Equations (57) and (2) gives

$$b = \left[\frac{2048\,(1-B_3)^2W_s(W_n+W_s)}{(1+B_3)W_n^2}\right]^{1/6} b_\delta \quad \ldots(77)$$

$$D_i = \frac{2}{\pi\rho V_\infty^2}\left[\frac{(1+B_3)W_n^2(W_n+W_s)^5}{2048\,(1-B_3)^2W_s b_\delta^6}\right]^{1/3}\left(1+\sum_{n=2}^{\infty}nB_n^2\right) \quad \ldots(78)$$

The allowable wingspans obtained from Equations (71), (73), (75), and (77) always increase with increasing wing-structure weight. However, the increase in wing-structure

https://doi.org/10.1017/aer.2020.24 Published online by Cambridge University Press

weight with respect to wingspan is greater for the deflection-limited solutions than for the stress-limited solutions. If the wingspan is low enough, the wing-structure weight required for the deflection-limited design is less than the wing-structure weight required for the stress-limited design, and the wing design will be stress limited. On the other hand, if the wingspan is high enough, the wing-structure weight required for the stress-limited design will be less than that required for the deflection-limited design, and the wing design will be deflection limited. For the case of fixed wing loading, combining Equations (71) and (73), the wing-structure weight that results when the wingspan is the same for both the stress-limited and deflection-limited designs is obtained from the relation

$$W_s = W_n \Bigg/ \left[\frac{32(C_\sigma \sigma_{\max})^2 (n_m + n_g)}{(1+B_3) C_\delta E \delta_{\max} \gamma \, n_m (n_g - 1)} - 1 \right] \qquad \ldots (79)$$

Similarly, for the case of fixed stall speed, combining Equations (75) and (77), the wing-structure weight that results when the wingspan for both the stress-limited and deflection-limited designs is the same is obtained from

$$W_s = W_n \Bigg/ \left[\frac{32 b_\sigma^6}{(1+B_3) b_\delta^6} - 1 \right] \qquad \ldots (80)$$

and after applying the definitions of b_σ and b_δ from Equations (38) and (55), we obtain

$$W_s = W_n \Bigg/ \left[\frac{32(C_\sigma \sigma_{\max})^2 (n_m + n_g)}{(1+B_3) C_\delta E \delta_{\max} \gamma \, n_m (n_g - 1)} - 1 \right]$$

which is identical to Equation (79) obtained for fixed wing loading. Because all acceptable designs must satisfy both the stress-limited and deflection-limited constraints, the wing-structure weight given by Equation (79) is an important parameter in this design space. Optimal designs resulting in a wing-structure weight less than that given by Equation (79) will be stress limited, and those resulting in a greater wing-structure weight will be deflection limited.

As an example of minimising induced drag with fixed net weight and wing loading, consider an airplane with a rectangular wing. The net weight is fixed at $W_n = 2600\text{lbf}$, and the wing loading is fixed at $W/S = 15\text{lbf/ft}^2$. To minimise the critical wing bending-moment distribution, the weight distributions given by Equations (5) and (6) are used. The typical manoeuvering-flight load limit for a civil aircraft is 2.5g. However, it is common to include a safety factor of 1.5 for the load limit. Therefore, in this example, we will use $n_m = n_g = 3.75$. Additional parameters for this design are $C_\sigma = 0.165$, $C_\delta = 0.653$, $t_{\max}/c = 0.12$, $\sigma_{\max} = 15.0 \times 10^3\text{psi}$, $\delta_{\max} = 4.5\text{ft}$, $\gamma = 0.10\text{lbf/in}^3$, $E = 10.0 \times 10^6\text{psi}$, $V_\infty = 200\text{ft/s}$, and $\rho = 0.0023769\text{slug/ft}^3$.

From this example, solutions for the wingspan and induced drag obtained from Equations (71)–(74) are shown in Fig. 3, plotted as a function of wing-structure weight for several different lift distributions. The lift distributions used to generate this figure are five of those shown in Fig. 1. The solution labels, a–e, used in Fig. 3 correspond to the lift-distribution labels used in Fig. 1. The solid curves in Fig. 3 correspond to the stress-limited solutions and the dashed curves are for the deflection-limited solutions. The black portion of each curve in Fig. 3 indicates the region where that solution provides the constraining limit. Each curve is shaded

https://doi.org/10.1017/aer.2020.24 Published online by Cambridge University Press

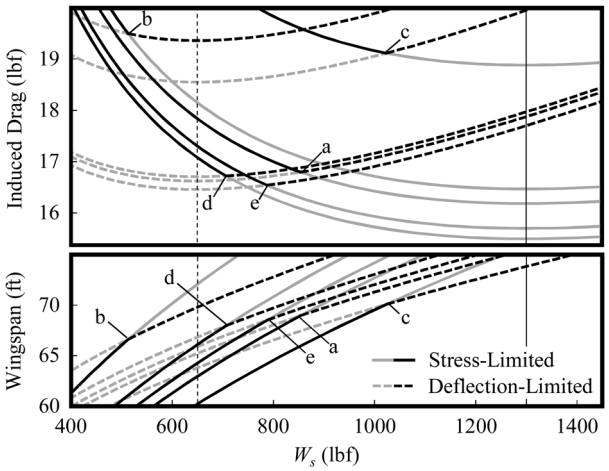

Figure 3. Wingspan and induced-drag solutions for the fixed-wing-loading example.

gray in the region where that solution does not provide the constraining limit. The solid vertical line shows the wing-structure weight $W_s = W_n/2$, which corresponds to the minimum induced drag for the stress-limited solutions as given in Equation (26). The dashed vertical line marks the wing-structure weight $W_s = W_n/4$, which gives minimum induced drag for the deflection-limited solutions as given in Equation (32).

Figure 3 illustrates the tradeoff between the stress-limited design and the deflection-limited design for this example. Notice from Fig. 3 that Prandtl's 1933 lift distribution (b) performs worse than the elliptic lift distribution (a), the lift distribution (c) produced by an untwisted rectangular wing, and the lift distributions (d) and (e), despite allowing the highest wingspan of the five lift distributions for any given wing-structure weight. This is, in part, because when Prandtl's 1933 lift distribution is used in conjunction with the wing parameters of this example, the design becomes deflection-limited at a lower wing-structure weight than any of the other four lift distributions. Prandtl's 1933 lift distribution gives minimum induced drag at $W_s = W_n/4$, which is the minimum-drag point on the deflection-limited curve. For this example, even an untwisted rectangular wing (c) has a lower minimum-drag point than that produced by Prandtl's 1933 lift distribution. However, the minimum-drag point for this lift distribution is not found at the minimum-drag point for either the stress-limited or deflection-limited curve. This lift distribution yields minimum induced drag at the wing-structure weight given by Equation (79), which is the point where the stress-limited curve crosses the deflection-limited curve. In fact, all lift distributions used to generate Fig. 3, except Prandtl's 1933 lift distribution, have minimum-drag points at the wing-structure weight given by Equation (79). If the wing-structure weight computed from Equation (79) is less than or equal to $W_s = W_n/4$, then minimum induced drag is always obtained at $W_s = W_n/4$. If the wing-structure weight computed from Equation (79) is greater than $W_s = W_n/4$ and less than $W_s = W_n/2$, then minimum induced drag is always obtained at the wing-structure weight computed from Equation (79). If the wing-structure weight computed from Equation (79) is greater than or equal to $W_s = W_n/2$, then minimum induced drag is always obtained at $W_s = W_n/2$.

Notice that the lowest minimum-drag point shown in Fig. 3 is for the lift distribution (e) given in Equation (18), which minimises induced drag for the deflection-limited solution.

https://doi.org/10.1017/aer.2020.24 Published online by Cambridge University Press

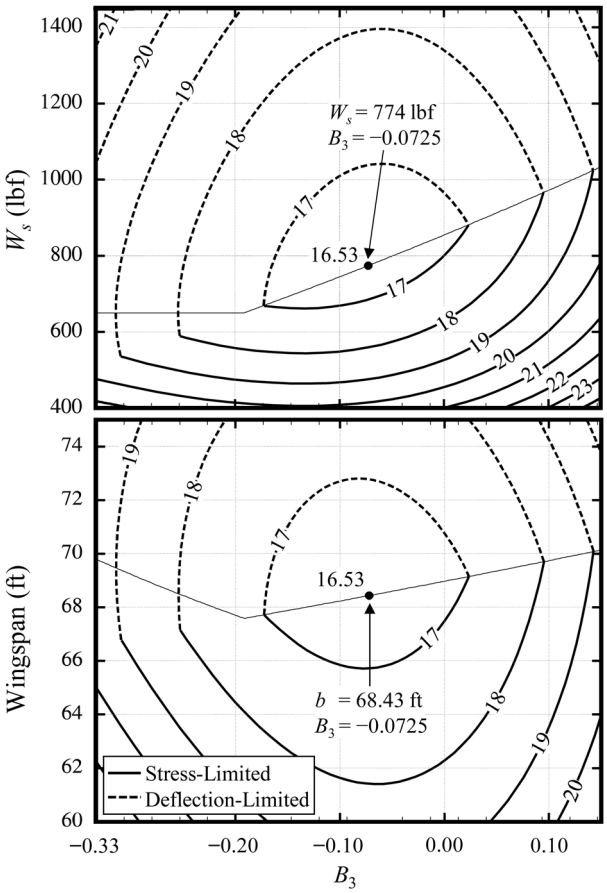

Figure 4. Constant induced-drag contours for the fixed-wing-loading example.

However, the lift distribution given in Equation (18) does not provide an absolute minimum in the induced drag for this example, because this minimum-drag point occurs at the wing-structure weight given by Equation (79). Using the wing-structure weight from Equation (79) in either Equation (72) or (74), together with the other parameters specified for this example, allows us to obtain the induced drag with $B_n = 0$ for all $n \neq 3$ as a function of the single design parameter B_3. The minimum in this function gives us the lift distribution and wing-structure weight that yield the absolute minimum induced drag for this example, i.e., $D_i = 16.53413$lbf at $B_3 = -0.07245516$ and $W_s = 774.1117$lbf. The wingspan for this optimal solution is $b = 68.43317$ft. For this example, this corresponds to an induced-drag coefficient of $C_{D_i} = 0.001546$ at a lift coefficient of $C_L = 0.3155$ and an aspect ratio of $R_A = 20.82$. Constant induced-drag contours for the design space near this optimal solution are shown in Fig. 4. It should be emphasised that the results shown in Figs. 3 and 4 are only valid for one example aircraft configuration. Different results may be obtained by changing any of the design parameters C_σ, C_δ, $t_{\max}/c$, $\sigma_{\max}$, $\delta_{\max}$, γ, or E, or by changing the design constraints.

As an example of minimising induced drag with fixed net weight and stall speed, consider an airplane with a rectangular wing. The net weight is fixed at $W_n = 2600$lbf, and the stall speed is fixed at $V_{\text{stall}} = 110$ft/s. Again we shall use the weight distributions given by

https://doi.org/10.1017/aer.2020.24 Published online by Cambridge University Press

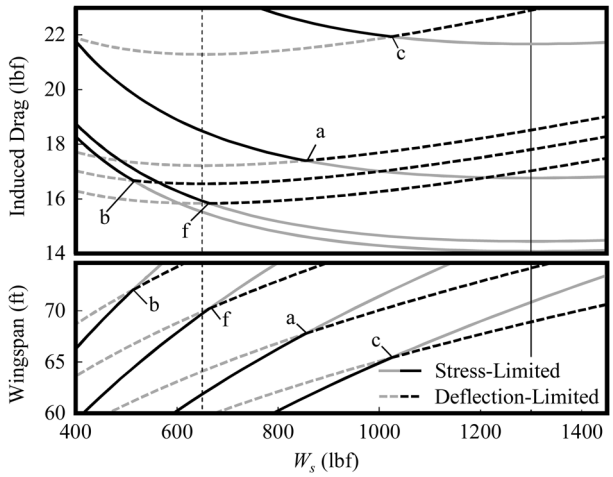

Figure 5. Wingspan and induced-drag solutions for the fixed-stall-speed example.

Equations (5) and (6) and the values $n_m = n_g = 3.75$, $C_\sigma = 0.165$, $C_\delta = 0.653$, $t_{\max}/c = 0.12$, $\sigma_{\max} = 15.0 \times 10^3$psi, $\delta_{\max} = 4.5$ft, $\gamma = 0.10$lbf/in^3, $E = 10.0 \times 10^6$psi, $V_\infty = 200$ft/s, and $\rho = 0.0023769$slug/ft^3.

Solutions for the wingspan and induced drag obtained from Equations (75)–(78) are shown in Fig. 5. The lift distributions used to generate this figure are four of those shown in Fig. 1. The labels, a–c and f, correspond to the lift-distribution labels used in Fig. 1. The solid curves correspond to the stress-limited solutions, and the dashed curves are for the deflection-limited solutions. The black portion of each curve indicates the region where that solution provides the constraining limit. Each curve is shaded grey in the region where that solution does not provide the constraining limit. The solid vertical line is the wing-structure weight $W_s = W_n/2$, which gives minimum induced drag for the stress-limited solutions as given in Equation (42). The dashed vertical line is the wing-structure weight $W_s = W_n/4$, which gives minimum induced drag for the deflection-limited solutions as given in Equation (60).

From Fig. 5 we see that for Prandtl's 1933 lift distribution (b), minimum induced drag is obtained at the minimum-drag point on the deflection-limited curve. All other lift distributions used in Fig. 5 have minimum-drag points at the wing-structure weight given by Equation (79), which is the point where the stress-limited curve crosses the deflection-limited curve. The lowest minimum-drag point shown in Fig. 5 is for the lift distribution (f) given in Equation (64), which minimises induced drag for the deflection-limited solution. However, the lift distribution given in Equation (64) does not provide an absolute minimum in the induced drag for this example, because this minimum-drag point occurs at the wing-structure weight given by Equation (79). Using the wing-structure weight from Equation (79) in either Equation (76) or (78), together with the other parameters specified for this example, we obtain the induced drag with $B_n = 0$ for all $n \neq 3$ as a function of the single design parameter B_3. The minimum in this function gives the lift distribution and wing-structure weight that yield the absolute minimum induced drag for this example, i.e., $D_i = 15.83315$lbf at $B_3 = -0.17889675$ and $W_s = 662.6372$lbf. The wingspan for this optimal solution is $b = 70.24208$ft. For this example, the optimal solution has an induced-drag coefficient of $C_{D_i} = 0.001369$ at a lift coefficient of $C_L = 0.2821$ and an aspect ratio of $R_A = 20.28$. Constant induced-drag contours for the design space near this optimal solution are shown in Fig. 6. Note from Figs. 4 and 6

https://doi.org/10.1017/aer.2020.24 Published online by Cambridge University Press

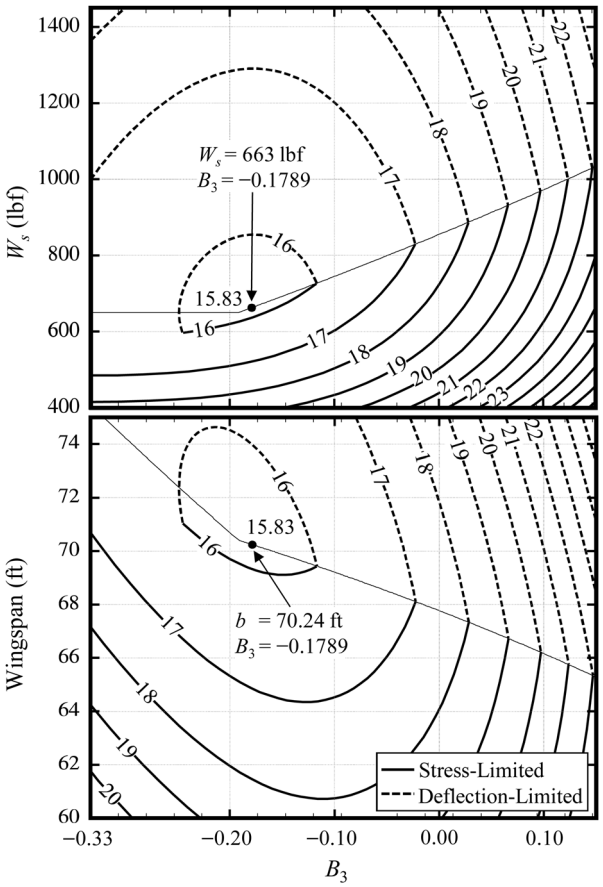

Figure 6. Constant induced-drag contours for the fixed-stall-speed example.

that for the range of B_3 values shown here, the optimum wingspan is either deflection-limited or follows Equation (79). In this way, the deflection limit discourages designs with excessive wingspans and excessive wingtip deflection.

It should be emphasised that the optimum solutions shown in Fig. 4 for the fixed-wing-loading example and in Fig. 6 for the fixed-stall-speed example are only valid for rectangular wings with the optimum net-weight distribution given by Equations (5) and (6). Figure 7 shows the net-weight distribution from Equation (5) as a function of the normalised spanwise coordinate for each of the example optimum solutions. In order to understand whether the optimum root weight and net-weight distribution are reasonable, it is helpful to compare them to those of an airframe that may have been optimised under similar constraints. A schematic of the spanwise fuel tank and engine layout in a Boeing 777 wing[74,75] is included in Fig. 7. Note that for this wing, the engine is located near the juncture of the inboard and outboard fuel tanks. For a transport aircraft such as the 777, fuel is first burned from the inboard tanks. Once the fuel in the inboard tanks is depleted, the fuel in the outboard tanks is used[76]. Due to wing dihedral, the fuel in the outboard tanks burns from the outboard regions first. Thus, as fuel is burned, the weight distribution tends to peak near the engine location. As shown in Fig. 7, the optimum weight distributions given by Equation (5) for the example optimum

https://doi.org/10.1017/aer.2020.24 Published online by Cambridge University Press

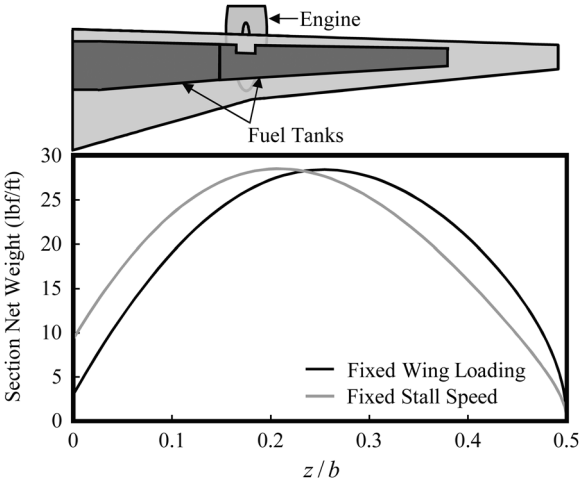

Figure 7. Net-weight distributions corresponding to the optimum solutions for the fixed-wing-loading and fixed-stall-speed examples.

solutions given in Figs 4 and 6 reasonably reflect this trend. At maximum takeoff weight, the Boeing 777 has a ratio of root weight to gross weight of about 0.44[75]. For sailplanes, this ratio typically ranges between about 0.35 and 0.72[72]. In the two examples shown above, $n_m = n_g = 3.75$. Applying this to Equation (6) results in an optimum ratio of root weight to gross weight of 0.37.

The reader is reminded that although the optimal net-weight distribution minimises the wing bending moments, it may not always be practical due to additional design constraints. Nevertheless, the solutions presented in this paper are valuable for understanding the aerodynamic and structural coupling involved in designing a wing for minimum induced drag, and the reader is reminded that results for tapered planforms do not deviate significantly from many of the solutions shown here[16].

6.0 CONCLUSIONS

As shown in Equation (2), Prandtl's classical lifting-line theory predicts that the induced drag acting on the wing of an airplane in steady level flight is directly proportional to the square of the ratio of gross weight to wingspan. For any fixed weight distribution and lift distribution, the critical wing section bending moments increase with increasing wingspan and the wing-structure weight required to support these bending moments also increases with wingspan. Hence, there exists an optimum wingspan and wing-structure weight that minimises the induced drag in steady level flight for any fixed net weight, weight distribution, and lift distribution. However, this optimum wingspan and wing-structure weight do not provide an absolute minimum in induced drag unless the optimum weight distribution and lift distribution are also used. The optimum weight distribution is obtained by enforcing both Equations (5) and (6). The optimum lift distribution depends on both the wing planform and the weight distribution. For the special case of a rectangular wing with spanwise-symmetric lift and the weight distribution specified by Equation (5), the optimum lift distribution is given by Equation (34) with $-1/3 \leq B_3 \leq 0$. The precise value of B_3 that provides the absolute minimum in induced drag depends on the design constraints.

https://doi.org/10.1017/aer.2020.24 Published online by Cambridge University Press

For any wing planform and wing structural design the wing-structure weight can be determined as a function of the wingspan, maximum allowable stress, maximum allowable deflection, and other design constraints. Because gross weight is the sum of the net weight and the wing-structure weight, for any wing design, the ratio of gross weight to wingspan can be written as $W/b = W_n/b + W_s/b$. For any fixed net weight, the term W_n/b always decreases with increasing wingspan; and for typical design constraints, the term W_s/b increases with increasing wingspan. Thus, for typical design constraints, there is an optimum wingspan that minimises the ratio of gross weight to wingspan based on the tradeoff between wingspan and wing-structure weight. Example analytic solutions that demonstrate this tradeoff are presented in the previous sections. It is shown that under certain constraints, induced-drag reductions in excess of 16% relative to a fixed elliptic lift distribution are possible.

Optimum solutions for two example wing designs are presented in the Results section. Figures 4 and 6 show how the induced drag varies with lift distribution, wingspan, and wing-structure weight near the optimum solution for each example. In each case, the optimum design produces a decrease in induced drag relative to the case of a fixed elliptic lift distribution.

For the analytic examples presented here, we have considered only rectangular wings with the optimum weight distribution specified by Equation (5). This provided the great simplification of allowing us to carry out the integration in Equation (9) for the arbitrary lift distribution given in Equation (1) to produce the analytic results for the wing-structure weights given in Equations (11) and (16). When the airfoil chord length and thickness vary with the spanwise coordinate, we can no longer use Equations (11) and (16) to compute the wing-structure weights for the stress-limited and deflection-limited solutions. Instead, we must return to the more general relation given in Equation (9). For arbitrary wing planforms and weight distributions, Equation (9) could be integrated numerically. Hence, for many practical applications, numerical methods may be required to obtain optimum lift distributions, wingspans, and wing-structure weights that minimise induced drag. Nevertheless, the analytic solutions presented in this work provide significant insight into the aerodynamic and structural coupling associated with designing wings for minimum induced drag.

ACKNOWLEDGEMENTS

This work was partially funded by the U.S. Office of Naval Research Sea-Based Aviation program, Grant No. N00014-18-1-2502, with Brian Holm-Hansen as the program officer. This work was also partially supported by the National Aeronautics and Space Administration under Grant No. 80NSSC18K1696 issued through the Aeronautics Research Mission Directorate through the 2018 NASA Fellowship Activity with Nhan Nguyen as the NASA Technical Advisor.

REFERENCES

1. PRANDTL, L. *Tragflügel Theorie, Nachricten von der Gesellschaft der Wissenschaften zu Güttingen*, Ges-chäeftliche Mitteilungen, Klasse, 1918, pp 451–477.
2. PRANDTL, L. Applications of modern hydrodynamics to aeronautics, NACA TR-116, June 1921.
3. PHILLIPS, W.F. Lifting-line analysis for twisted wings and washout-optimized wings, *J Aircr*, 2004, **41**, (1), pp 128–136. (doi:10.2514/1.262)

4. PHILLIPS, W.F., ALLEY, N.R. and GOODRICH, W.D. Lifting-line analysis of roll control and variable twist, *J Aircr*, 2004, **41**, (5), pp 1169–1176. (doi:10.2514/1.3846)
5. PHILLIPS, W.F. New twist on an old wing theory, *Aerospace America*, 2005, pp 27–30.
6. PHILLIPS, W.F., FUGAL, S.R. and SPALL, R.E. Minimizing induced drag with wing twist, computational-fluid-dynamics validation, *J Aircr*, 2006, **43**, (2), pp 437–444. (doi:10.2514/1.15089)
7. PHILLIPS, W.F. and ALLEY, N.R. Predicting maximum lift coefficient for twisted wings using lifting-line theory, *J Aircr*, 2007, **44**, (3), pp 898–910. (doi:10.2514/1.25640)
8. PHILLIPS, W.F. Incompressible Flow over Finite Wings, *Mechanics of Flight*, 2nd ed., Wiley, 2010, Hoboken, NJ, pp 46–94.
9. PHILLIPS, W.F., HUNSAKER, D.F. and JOO, J.J. Minimizing induced drag with lift distribution and wingspan, *J Aircr*, 2019, **56**, (2), pp 431–441. (doi:10.2514/1.C035027)
10. PRANDTL, L. Über Tragflügel kleinsten induzierten Widerstandes, *Zeitschrift für Flugtechnik und Motorluftschiffahrt*, 1933, **24**, (11), pp 305–306.
11. HUNSAKER, D.F. and PHILLIPS, W.F. Ludwig Prandtl's 1933 Paper Concerning Wings for Minimum Induced Drag, Translation and Commentary, AIAA SciTech 2020 Forum, Orlando, Florida, 6–10 January 2020.
12. JONES, R.T. The Spanwise Distribution of Lift for Minimum Induced Drag of Wings Having a Given Lift and a Given Bending Moment, NACA TR-2249, December 1950.
13. JONES, R.T. and LASINSKI, T.A. Effect of Winglets on the Induced Drag of Ideal Wing Shapes, NASA TM-81230, September 1980.
14. KLEIN, A. and VISWANATHAN, S.P. Minimum induced drag of wings with given lift and root-bending moment, *Zeitschrift fur Angewandte Mathematik und Physik*, 1973, **24**, pp 886–892.
15. KLEIN, A. and VISWANATHAN, S.P. Approximate solution for minimum induced drag of wings with given structural weight, *J Aircr*, 1975, **12**, (2), pp 124–126. (doi:10.2514/3.44425)
16. TAYLOR, J.D. and HUNSAKER D.F. Minimum Induced Drag for Tapered Wings Including Structural Constraints, AIAA-2020-2113, AIAA Scitech 2020 Forum, Orlando, Florida, 6–10 January, 2020. (doi:10.2514/6.2020-2113)
17. LUNDRY, J.L. Minimum swept-wing induced drag with constraints on lift and pitching moment, *J Aircr*, 1967, **4**, pp 73–74. (doi:10.2514/3.43797)
18. LISSAMAN, P.B.S. and LUNDRY, J.L. A numerical solution for the minimum induced drag of nonplanar wings, *J Aircr*, 1968, **5**, pp 17–21. (doi:10.2514/3.43901)
19. ASHENBERG, J. and WEIHSRADIUS, D. Minimum induced drag of wings with curved planform, *J Aircr*, 1984, **21**, pp 89–91. (doi:10.2514/3.56733)
20. MCGEER, T. Wing design for minimum drag with practical constraints, *J Aircr*, 1984, **21**, pp 879–886. (doi:10.2514/3.45058)
21. ROKHSAZ, K. Effect of viscous drag on optimum spanwise lift distribution, *J Aircr*, 1993, **30**, pp 152–154. (doi:10.2514/3.46328)
22. DEMASI, L. Induced drag minimization: a variational approach using the acceleration potential, *J Aircr*, 2006, **43**, pp 669–680. (doi:10.2514/1.15982)
23. DEMASI, L. Erratum on induced drag minimization: a variational approach using the acceleration potential, *J Aircr*, 2006, **43**, p 1247. (doi:10.2514/1.26648)
24. DEMASI, L. Investigation on the conditions of minimum induced drag of closed wing systems and C-wings, *J Aircr*, 2007, **44**, pp 81–99. (doi:10.2514/1.21884)
25. PATE, D.J. and GERMAN, B.J. Lift distributions for minimum induced drag with generalized bending moment constraints, *J Aircr*, 2013, **50**, pp 936–946. (doi:10.2514/1.C032074)
26. DEMASI, L., DIPACE, A., MONEGATO, G. and CAVALLARO, R. Invariant formulation for the minimum induced drag conditions of nonplanar wing systems, *AIAA J*, 2014, **52**, pp 2223–2240. (doi:10.2514/1.J052837)
27. WROBLEWSKI, G.E. and ANSELL, P.J. Prediction and experimental evaluation of planar wing spanloads for minimum drag, *J Aircr*, 2017, **54**, pp 1664–1674. (doi:10.2514/1.C034156)
28. DEMASI, L., MONEGATO, G. and CAVALLARO, R. Minimum Induced Drag Theorems for Multiwing Systems, *AIAA J*, 2017, **55**, pp 3266–3287. (doi:10.2514/1.J055652)
29. NOLL, T.E., ISHMAEL, S.D., HENWOOD, B., PEREZ-DAVIS, M.E., TIFFANY, G.C., MADURA, J., GAIER, M., BROWN, J.M. and WIERZBANOWSKI, T. Technical Findings, Lessons Learned, and Recommendations Resulting from the Helios Prototype Vehicle Mishap, NATO/RTO AVT-145 Workshop on Design Concepts, Processes, and Criteria for UAV Structural Integrity, Florence, Italy, 14–18 May, 2007.

30. VOS, R., GURDAL, Z. and ABDALLA, M. Mechanism for warp-controlled twist of a morphing wing, *J Aircr*, 2010, **47**, (2), pp 450–457. (doi:10.2514/1.39828)
31. JOO, J., MARKS, C., ZIENTARSKI, L. and CULLER, A. Variable camber compliant wing – design, AIAA-2015-1050, 23rd AIAA/AHS Adaptive Structures Conference, Kissimmee, Florida, 5–9 January 2015.
32. MARKS, C.R., ZIENTARSKI, L., CULLER, A.J., HAGEN, B., SMYERS, B.M. and JOO, J.J. Variable camber compliant wing – wind tunnel testing", AIAA 2015-1051, 23rd AIAA/AHS Adaptive Structures Conference, Kissimmee, Florida, 5–9 January, 2015.
33. MILLER, S.C., RUMPFKEIL, M.P. and JOO, J.J. Fluid-structure interaction of a variable camber compliant wing, AIAA-2015-1235, 53rd AIAA Aerospace Sciences Meeting, Kissimmee, Florida, 5–9 January 2015.
34. JOO, J.J., MARKS, C.R. and ZIENTARSKI, L. Active wing shape reconfiguration using a variable camber compliant wing system, 20th International Conference on Composite Materials, Copenhagen, Denmark, 19–24 July 2015.
35. MARKS, C.R., ZIENTARSKI, L. and JOO, J.J. Investigation into the effect of shape deviation on variable camber compliant wing performance, AIAA-2016-1313, 24th AIAA/AHS Adaptive Structures Conference, San Diego, California, 4–8 January 2016.
36. ALLEY, N.R., PHILLIPS, W.F. and SPALL, R.E. Predicting maximum lift coefficient for twisted wings using computational fluid dynamics, *J Aircr*, 2007, **44**, (3), pp 911–917. (doi:10.2514/1.25643)
37. VERNENGO, G., BONFIGLIO, L. and BRIZZOLARA, S. Supercavitating three-dimensional hydrofoil analysis by viscous lifting-line approach, *AIAA J*, 2017, **55**, (12), pp 4127–4141. (doi:10.2514/1.J055504)
38. GAMBLE, L.L., PANKONIEN, A.M. and INMAN, D.J. Stall recovery of a morphing wing via extended nonlinear lifting-line theory, *AIAA J*, 2017, **55**, (9), pp 2956–2963. (doi:10.2514/1.J055042)
39. IZRAELEVITZ, J.S., ZHU, Q. and TRIANTAFYLLOU, M.S. State-space adaptation of unsteady lifting line theory: twisting/flapping wings of finite span, *AIAA J*, 2017, **55**, (4), pp 1279–1294. (doi:10.2514/1.J055144)
40. GALLAY, S. and LAURENDEAU, E. Preliminary-design aerodynamic model for complex configurations using lifting-line coupling algorithm, *J Aircr*, 2016, **53**, (4), pp 1145–1159. (doi:10.2514/1.C033460)
41. GALLAY, S. and LAURENDEAU, E. Nonlinear generalized lifting-line coupling algorithms for pre/poststall flows, *AIAA J*, 2015, **53**, (7), pp 1784–1792. (doi:10.2514/1.J053530)
42. SPALART, P.R. Prediction of lift cells for stalling wings by lifting-line theory, *AIAA J*, 2014, **52**, (8), pp 1817–1821. (doi:10.2514/1.J053135)
43. PHILLIPS, W.F. Analytical decomposition of wing roll and flapping using lifting-line theory, *J Aircr*, 2014, **51**, (3), pp 761–778. (doi:10.2514/1.C032399)
44. PHILLIPS, W.F. and HUNSAKER, D.F. Lifting-line predictions for induced drag and lift in ground effect, *J Aircr*, 2013, **50**, (4), pp 1226–1233. (doi:10.2514/1.C032152)
45. WICKENHEISER, A.M. and GARCIA, E. Extended nonlinear lifting-line method for aerodynamic modeling of reconfigurable aircraft, *J Aircr*, 2011, **48**, (5), pp 1812–1817. (doi:10.2514/1.C031406)
46. JUNGE, T., GERHARDT, F.C., RICHARDS, P. and FLAY, R.G.J. Optimizing spanwise lift distributions yacht sails using extended lifting line analysis, *J Aircr*, 2010, **47**, (6), pp 2119–2129. (doi:10.2514/1.C001011)
47. WICKENHEISER, A. and GARCIA, E. Aerodynamic modeling of morphing wings using an extended lifting-line analysis, *J Aircr*, 2007, **44**, (1), pp 10–16. (doi:10.2514/1.18323)
48. SUGIMOTO, T. Induced velocity in the plane of an elliptically loaded lifting line, *AIAA J*, 2002, **40**, (6), pp 1233–1236. (doi:10.2514/2.1776)
49. PHILLIPS, W.F. and SNYDER, D.O. Modern adaptation of prandtl's classic lifting-line theory, *J Aircr*, 2000, **37**, (4), pp 662–670. (doi:10.2514/2.2649)
50. RASMUSSEN, M.L. and SMITH, D.E. Lifting-line theory for arbitrarily shaped wings, *J Aircr*, 1999, **36**, (2), pp 340–348. (doi:10.2514/2.2463)
51. IOSILEVSKII, G. Lifting-line theory of an arched wing in asymmetric flight, *J Aircr*, 1996, **33**, (5), pp 1023–1026. (doi:10.2514/3.47050)
52. JADIC, I. and CONSTANTINESCU, V.N. Lifting line theory for supersonic flow applications, *AIAA J*, 1993, **31**, (6), pp 987–994. (doi:10.2514/3.11718)
53. PLOTKIN, A. and TAN, C.H. Lifting-line solution for a symmetrical thin wing in ground effect, *AIAA J*, 1986, **24**, (7), pp 1193–1194. (doi:10.2514/3.9413)

54. CHENG, H.K., MENG, S.Y., CHOW, R. and SMITH, R.C. Transonic swept wings studied by the lifting-line theory, *AIAA J*, 1981, **19**, (8), pp 961–968. (doi:10.2514/3.7837)
55. ANDERSON, J.D. and CORDA, S. Numerical lifting line theory applied to drooped leading-edge wings below and above stall, *J Aircr*, 1980, **17**, (12), pp 898–904. (doi:10.2514/3.44690)
56. CHENG, H.K. and MENG, S.Y. Lifting-line theory of oblique wings in transonic flows, *AIAA J*, 1979, **17**, (1), pp 121–124. (doi:10.2514/3.61081)
57. CHENG, H.K. Lifting-line theory of oblique wings, *AIAA J*, 1978, **16**, (11), pp 1211–1213. (doi:10.2514/3.61033)
58. SMALL, R.D. Transonic lifting line theory - Numerical procedure for shock-free flows, *AIAA J*, 1978, **16**, (6), pp 632–634. (doi:10.2514/3.7562)
59. LAN, C.E. and FASCE, M.H. Applications of an improved nonlinear lifting-line theory, *J Aircr*, 1977, **14**, (4), pp 404–407. (doi:10.2514/3.44601)
60. BERA, R.K. Comment on "Solution of the Lifting Line Equation for Twisted Elliptic Wings", *J Aircr*, 1975,**12**, (6), pp 561–562. (doi:10.2514/3.59834)
61. BERA, R.K. Some remarks on the solution of the lifting line equation, *J Aircr*, 1974, **11**, (10), pp 647–648. (doi:10.2514/3.44397)
62. LAN, C.T. An improved nonlinear lifting-line theory, *AIAA J*, 1973, **11**, (5), pp 739–742. (doi:10.2514/3.6819)
63. KERNEY, K.P. A correction to 'lifting-line theory as a singular perturbation problem', *AIAA J*, 1972, **10**, (12), pp 1683–1684. (doi:10.2514/3.6702)
64. FILOTAS, L.T. Solution of the lifting line equation for twisted elliptic wings, *J Aircr*, 1971, **8**, (10), pp 835–836. (doi:10.2514/3.44308).
65. LAKSHMINARAYANA, B. Extension of lifting-line theory to a cascade of split aerofoils, *AIAA J*, 1964, **2**, (5), pp 938–940. (doi:10.2514/3.2461)
66. ANDERSON, R.C. and MILLSAPS, K. Application of the galerkin method to the prandtl lifting line equation, *J Aircr*, 1964, **1**, (3), pp 126–128. (doi:10.2514/3.43565)
67. TUYL, A.V. The replacement of lifting surfaces by lifting lines with variable position, *J Aerospace Sciences*, 1959, **26**, (2), pp 127–128. (doi:10.2514/8.7967)
68. DENGLER, M.A. Concerning "The subsonic calculation of circulatory spanwise loadings for oscillating airfoils by lifting-line techniques", *J Aeronautical Sciences*, 1953, **20**, (6), pp 439–439. (doi:10.2514/8.2673)
69. DENGLER, M.A. The subsonic calculation of circulatory spanwise loadings for oscillating airfoils by lifting-line techniques, *J Aeronautical Sciences*, 1952, **19**, (11), pp 751–759. (doi:10.2514/8.2459)
70. REISSNER, E. Note on the relation of lifting-line theory to lifting-surface theory, *J Aeronautical Sciences*, 1951, **18**, (3), pp 212–214. (doi:10.2514/8.1905)
71. FLAX, A.H. On a variational principle in lifting-line theory, *J Aeronautical Sciences*, 1950, **17**, (9), pp 596–597. (doi:10.2514/8.1732)
72. THOMAS, F. Appendix 1: Sailplane Design Data and Drawings, *Fundamentals of Sailplane Design*, Translated by J. MILGRAM, College Park Press, College Park, MD, 1999, pp 195–244.
73. STEWART, A.J. and HUNSAKER, D.F. Minimization of Induced and Parasitic Drag on Variable-Camber Morphing Wings, AIAA-2020-0277, AIAA Scitech 2020 Forum, Orlando, Florida, 6–10 January, 2020. (doi:10.2514/6.2020-0277)
74. Boeing 777 Airplane Rescue and Fire Fighting Information, Boeing Commercial Airplanes, October, 2018.
75. 777-200/300 Airplane Characteristics for Airport Planning, D6-58329, Boeing Commercial Airplanes, July, 1998.
76. LANGTON, R., CLARK, C., HEWITT, M. and RICHARDS, L. Fuel System Functions of Commercial Aircraft, *Aircraft Fuel Systems*, Wiley, Hoboken, NJ, 2009, pp 53–95. (doi: 10.1002/9780470059470)